

# **3-D geophysical inversion-modeling and intrusion estimation using gravity data of convergence zone between Pan-African-belt and Congo Craton, Centre-South of Cameroon: its geothermal implications on limit between the two geotectonic units**

*Alain Narcisse S. Feumoe*<sup>a,b,\*</sup>, *Marcelin Pemi Mouzong*<sup>c,d</sup>, and *Evariste H. Ngatchou*<sup>e</sup>

<sup>a</sup>Department of Civil Engineering and Architectural Engineering, Faculty of Engineering and Technology, University of Buéa, P.O. Box 63, Buéa-Cameroon

<sup>b</sup>Bureau de Recherches d'Etudes et de Contrôles Géotechniques (B.R.E.C.G), PO Box 7883 Yaoundé, Cameroon

<sup>c</sup>Department of Renewable Energy, Higher Technical Teachers' Training College, University of Buéa, P.O. Box 249 Buéa, Cameroon

<sup>d</sup>Department of Basic sciences, University Institute of Technology, University of Douala, P.O. Box 8698, Douala, Cameroon

<sup>e</sup>Department of Physics, Advanced Teacher's Training College, University of Yaoundé 1, P.O. Box 47, Yaoundé, Cameroon

\*Corresponding author: [alainfeumoe@yahoo.fr](mailto:alainfeumoe@yahoo.fr)

(Submitted: 2022-03-08; Accepted: 2022-10-15; Final form: 2023-02-18)

## *Abstract*

*Geothermal energy resources of the northern part of Congo Craton boundary in Cameroon are highlighted by 3-D geophysical inversion-modeling and intrusion estimation using gravity data. Determination of the magnitude maxima of (1) tilt derivative gravity allowed map to be produced showing various lines of fractures interpreted as the preferential paths for circulation of geothermal energy resources up flow to the surface, and (2) the total horizontal derivative give an overview of the possible deep geological setting in the area, which are acting as the source of geothermal potential. We find that these structures (fractures and igneous intrusion) are associated to long-wavelength anomalies, suggesting that its should be connected with large-scale structural deformation due to the collision between Congo Craton (CC) and Pan-African belt or Mobile zone (MZ). Interpretation of 3-D density models derived from the inversion of gravity data shows the presence of igneous intrusion within the faults with high density, probably granulitic rocks put in place during the Pan-African belt reactivation. The distribution of high density constitutes the geothermal potential energy resources of the studied area.*

*Keywords: Bouguer anomaly; tilt derivative gravity; 3-D analytic signal amplitude; density modeling; geotectonic units*

## *1 Introduction*

The measured gravity field is caused mainly by the gravitational attraction of Earth's mass, but it is also affected by the centrifugal force due to Earth's rotation and the ellipsoidal shape of the Earth. The international gravity formula (IGF) defines the normal value of the gravity on a reference ellipsoid, the surface of which coincides with the mean sea level of the oceans (*Choi et al.*, 2019; *Geng et al.*, 2019a,b, 2020; *Ghomsi et al.*, 2020).

The gravity field is not uniform, because the mass is not uniformly distributed inside the Earth. Large scale anomalies in the gravity field and the potential defined by the geoid are caused by mass variations inside Earth's crust and mantle. Local anomalies that are usually studied in applied geophysics are caused by topography variations and near-surface mass distributions (Telford *et al.*, 1990; Pirttijärvi, 2014). Geophysical investigations carried out in the northern edge of Congo Craton in southern Cameroon have used seismic, gravimetric, magnetic and magneto-telluric methods to study deep and superficial structures, to propose geodynamic and tectonic evolutionary models for the region (Manguelle Dicoum *et al.*, 1992; Mbom-Abane, 1997; Tadjou *et al.*, 2004, 2009; Shandini *et al.*, 2010; Tokam *et al.*, 2010; Shandini *et al.*, 2011; Ndougsa-Mbarga *et al.*, 2012; Feumoe *et al.*, 2012; Feumoe, 2014; Feumoe and Ndougsa-Mbarga, 2017). The results obtained suggest that (1) the area was affected by a series of tectonic events due to the collision between the Pan-African belt and Congo Craton that formed the structural features of the southern Cameroon, (2) the depth of the Moho is between 48 km and 50 km, and (3) the Curie point depth of magnetic sources does not exceed 25 km. The purpose of this study, based on the 3-D geophysical inversion-modeling and intrusion estimation using gravity data, is to obtain knowledge of the deep structure in the area, and to analyse the geothermal potential resources over an area comprised between longitudes 10.50°E and 16.50°E and latitudes 3.50°N and 6.00°N by considering the existing geophysical and geological information. This is made possible by the magnitude maxima of tilt derivative gravity (Miller and Singh, 1994; Cooper and Cowan, 2006), the total horizontal derivative developed by Nabighian (1974) and Roest *et al.* (1992) as well as 3-D modeling and inversion of gravity sources. Many authors, e.g., Pirttijärvi (2014), Farhi *et al.* (2016), Andersson and Malehmir (2018), Choi *et al.* (2019), and Geng *et al.* (2019a,b, 2020) have demonstrated the effectiveness of these techniques in mapping of crustal fabric, basement structures, intrusive complexes, rift basins and particularly the distribution of high density beneath the cover. These methods are used here to highlight and characterize the structural features, igneous intrusion, and distribution of high density in the study area. As the results approve the effectiveness of these methods, to test this aspect of the gravity analysis results, we constructed four vertical models across the zone of collision each of one west-east trending direction and three south-north-trending direction. The results are assessed and give an overview of the possible deep geological setting in the area which explain the occurrence of high density at depth, sources of geothermal energy resources. The study is organized into many sections. Section 2 describes the geological and tectonic setting of the study area, data acquisition and interpretation of the Bouguer anomaly map is given in Section 3. The methods we used to proceed are briefly described in Section 4, the results are presented and interpreted in Sections 5 and 6. The study is concluded in Section 7.

## 2 Geologic and tectonic setting

Geologically, the area studied includes the Pan African Belt (Yaoundé Domain) and Congo Craton with its Proterozoic cover (lower Dja serie), which has a complex structure (Fig. 2.1).

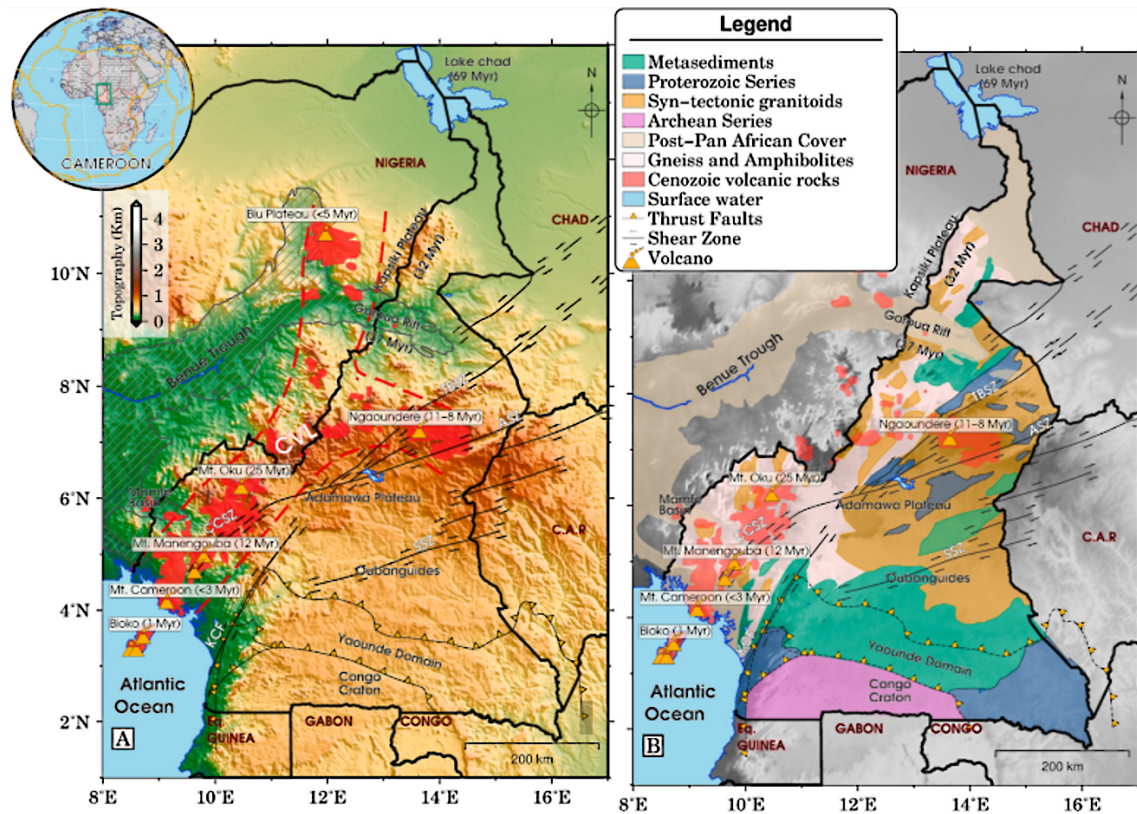


Fig. 2.1: Simplified (a) topographic map and (b) structural and tectonic map of Cameroon (modified after Ghomsi *et al.*, 2020).

The Yaoundé domain (YD) is the southernmost part of the Oubangui complex (Poidevin, 1983; Ngako *et al.*, 2003; Owona *et al.*, 2012) which is the southern part of the Central African Fold Belt (CAFB) formed during the collision of Congo, West African and East Sahara cratons during the Pan-African orogeny ( $\sim 600$  Ma; e.g., Abdelsalam *et al.*, 2002; Ngako *et al.*, 2003; Owona *et al.*, 2012). This domain is interpreted as an allochthonous nappe thrust onto the autochthonous Congo craton. The YD is made up of low-to high-grade garnet-bearing schist, orthogneisses and gneisses (Fig. 2.2), which had been subjected to medium-high pressure metamorphism reaching the granulite facies (Toteu *et al.*, 2004). In the study area, the YD consists of the series known as ‘intermediate series’. The Mbalmayo–Bengbis series are dominated by schist and quartzites which recrystallized in the greenschist facies conditions (Vicat, 1998). The Yaoundé series consists of strongly deformed metamorphic rocks (schists and gneisses) and migmatites (Nzenti *et al.*, 1988). Isotopic data from Toteu *et al.* (1994) and Toteu *et al.* (2001) indicate that the metaigneous and metasedimentary rocks originated from a protolith made up of a mixture of juvenile Paleoproterozoic and Neoproterozoic sources without noticeable contribution from the Congo craton. The only possible source for old components is illustrated by the Paleoproterozoic basement of north-central Cameroon, which suggests that the Yaoundé series were formed in the internal zone of the mobile belt before the southward thrusting onto the Congo craton (Toteu *et al.*, 2004).

The Craton constitutes the north-western part of the Congo Craton and is very well

Coordinate System: GCS WGS 1984  
 Datum: WGS 1984  
 Units: Degree

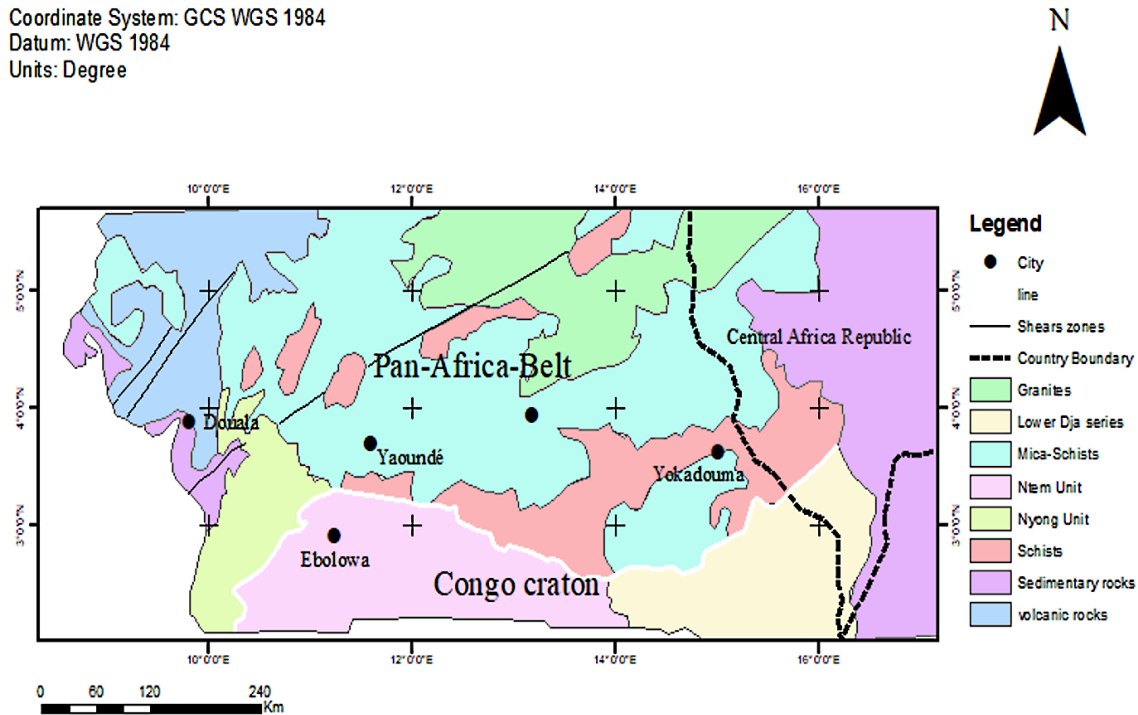


Fig. 2.2: Geological sketch map of the studied area, showing the two distinct geotectonic units PAB and CC. Modified after *Soba, 1989* and *Poidevin, 1991*.

exposed in southern Cameroon (*Maurizot et al., 1986*). It includes Ntem unit and Lower Dja series (Proterozoic cover). The Ntem unit is made up dominantly of Archean rocks with some reworked material that formed in Early Proterozoic times (*Tchameni et al., 2000; Tchameni, 2001*).

The Pan-African units rest directly on the Ntem complex basement and constitute the second cover of the Congo Craton. The first Craton cover (Proterozoic) is constituted by the Dja series and the tillitic complexes. It is discordant with the Mbalam belt and covered partially in the north by the Yaoundé nappe (*Mvondo et al., 2003; Caron et al., 2010*).

The major tectonic feature of the region is constituted by the extension of the Congo Craton under the Pan-African units. This event marks the subduction of the Congo Craton under the Pan-African belt. According to the hypothesis of subduction of the southern plate Craton, it must have provoked deep fractures in covers.

### 3 Gravity anomaly and interpretation of Bouguer map

#### 3.1 The origin of gravity data

The gravity data used in this work were obtained from the Office de la Recherche Scientifique et Technique d'Outre-Mer (ORSTOM) database. The data were collected in the area, using Worden gravimeters (no. 69, 135, 313, and 600), 0.2 mGal/division scale precision and Lacoste & Romberg gravimeters (model G no. 471 and 823). The altimeter readings were looped along with gravimeter reading to obtain reliable height differences

between base stations, thereby guaranteeing reasonably accurate elevation values for intermediates stations. Maximum error in determining the height of any station by means of altimeters did not exceed 10 m. Consequently, Bouguer anomaly value maximum error for any station due to the above height determination error was not expected to exceed 0.15 mGal. The Bouguer anomaly values resulted from free-air reduction referring to the ellipsoid, infinite plate reduction with  $2.670 \text{ g cm}^{-3}$  constant reduction density and topographic reduction (Crenn, 1967; Collignon, 1968). Gravity survey accuracy was estimated to be about  $\pm 0.5 \text{ mGal}$ .

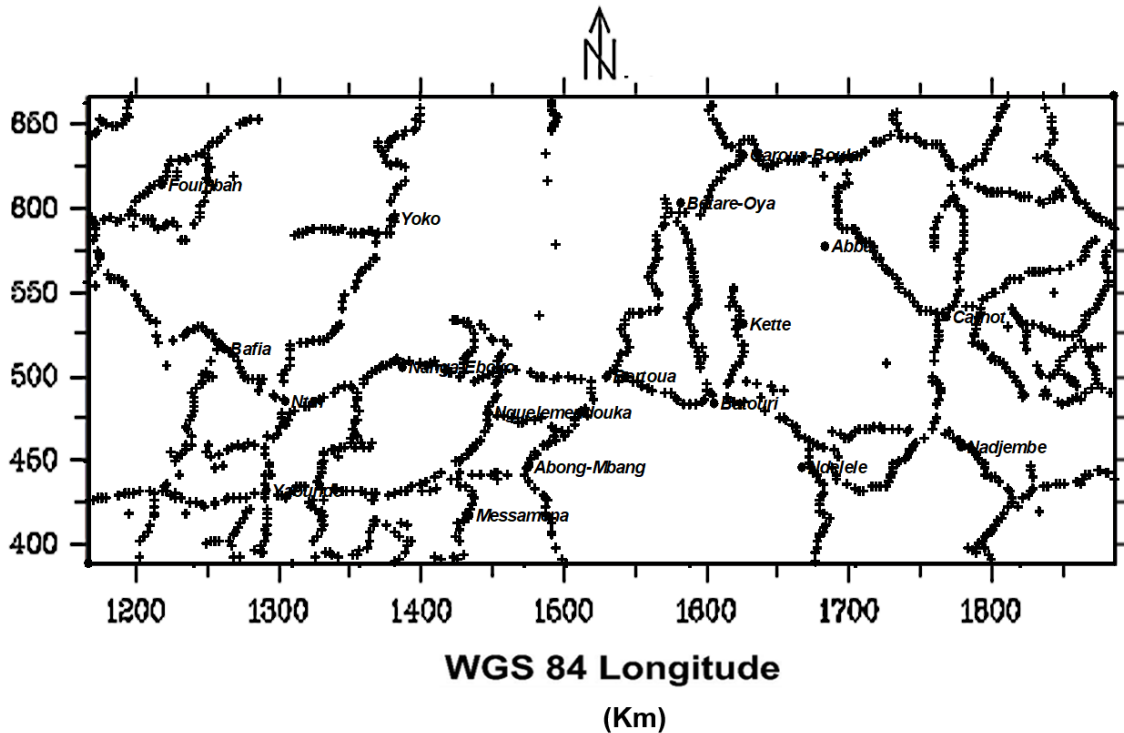


Fig. 3.1: Map showing the distribution of interpreted gravity data in the area being studied.

### 3.2 Bouguer anomaly map

This map (Fig. 3.2) shows that the region is characterized by a broad anomaly ranging from  $-110 \text{ mGal}$  to  $-20 \text{ mGal}$  and bounded by relative steep gradients. The map is characterized by high frequencies of anomalies and shows an acute variation in the gravity density, indicating variations in either lithology or basement topography. The presence of high gravity anomaly coupled with steep gradients which occur in the southern part suggests the existence of a suture zone between two different density blocks of the crust (Kennedy, 1984; Shandini *et al.*, 2010). We find that these structures are associated to long-wavelength anomalies, suggesting that its should be connected with large-scale structural deformation due to the collision between Congo Craton (CC) and Pan-African belt or Mobile zone (MZ). The map shows a relative gravity magnitude greater than  $-20 \text{ mGal}$  situated on an axis, which has a WNW–ESE direction. This gravity magnitude could be probably due to possible deep geological setting in the study area.

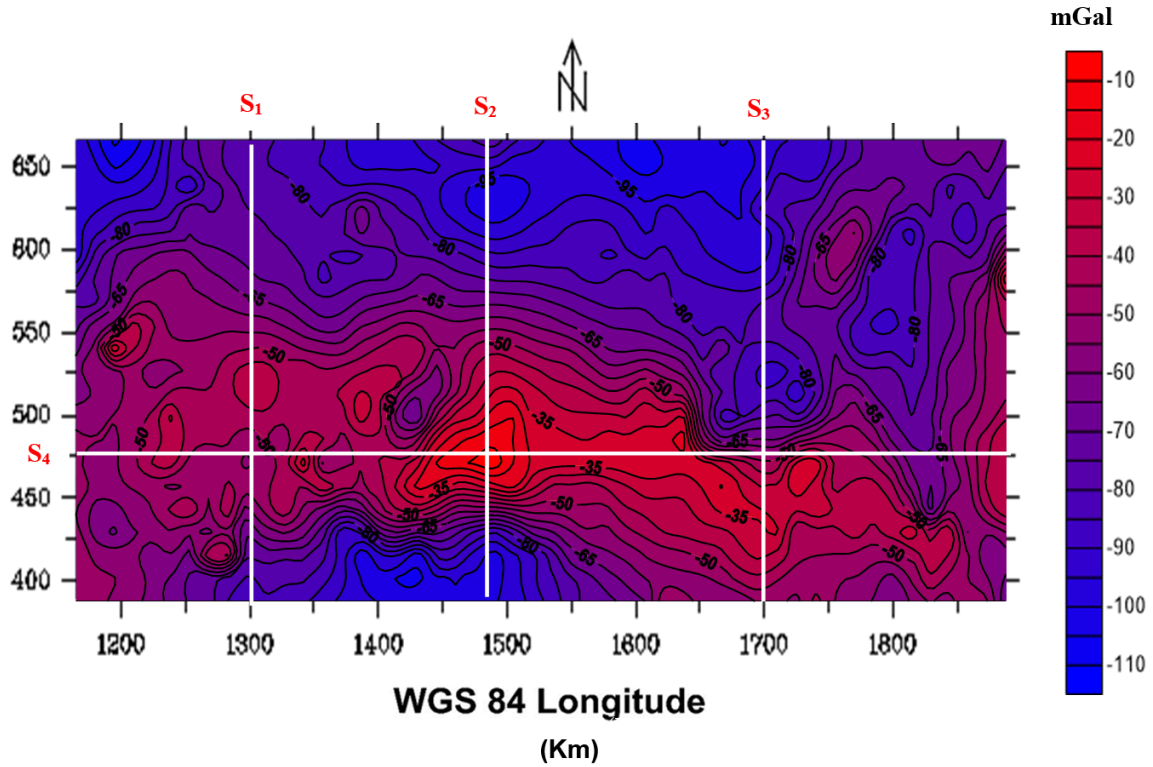


Fig. 3.2: Bouguer anomaly map of the study area (Intervals: 5 mGal) showing studied profiles for 3-D density model. ( $S_1$ ,  $S_2$  and  $S_3$  directed south-north and  $S_4$  directed west-east).

#### 4 Data processing methods

The methodologies we used to proceed with the geologic and gravity interpretation are discussed in this section. These approaches are (1) tilt derivatives gravity, (2) the total horizontal gradient and (3) 3-D modeling and inversion of gravity sources. These methods are briefly described as following.

##### 4.1 Derivatives gravity

Horizontal derivatives of gravity field data were computed using finite differences relations. At a grid point  $i, j$  the derivatives of a gravity anomaly field measurement value  $g_{i,j}$  in the  $x$  and  $y$  directions are given as:

$$\begin{aligned}\frac{\partial g}{\partial x} &= \frac{g_{i+1,j} - g_{i-1,j}}{2\Delta x} \\ \frac{\partial g}{\partial y} &= \frac{g_{i,j+1} - g_{i,j-1}}{2\Delta y}\end{aligned}\quad (4.1)$$

The derivative of the gravity field data in the vertical direction can be computed in the frequency environment using the equation below (Gunn, 1975):

$$\frac{\partial g}{\partial z} = g(f)|f| \quad (4.2)$$

Here  $\partial g/\partial x$ ;  $\partial g/\partial y$ ;  $\partial g/\partial z$  are first vertical derivatives of the gravity field in  $x$ ,  $y$  and  $z$  directions.  $g(f)$  shows the amplitude value in the  $f$  frequency.

#### 4.1.1 Tilt derivatives gravity

Tilt derivative gravity (TDR) edge detection on gravity data is a common technique in geophysical interpretation, which is able to detect faults through significant density contrast. It is a potential field data processing technique which is adequate to detect edges of structural bodies by edge enhancement. In this study, this method was used to highlight the deep faults system which is assumed to be the preferential paths as the circulation of geothermal energy resources up flow to the surface (Nouraliee *et al.*, 2015; Moghaddam *et al.*, 2016). Tilt derivative is defined as the arc-tangent value of the ratio of the vertical derivative of the potential field to its horizontal derivative. If  $g$  is the gravity anomaly field, then the tilt derivative gravity is given by (Miller and Singh, 1994; Verduzco *et al.*, 2004; Cooper and Cowan, 2006):

$$\text{TDR} = \tan^{-1} \left( \frac{\frac{\partial g}{\partial z}}{\sqrt{\left(\frac{\partial g}{\partial x}\right)^2 + \left(\frac{\partial g}{\partial y}\right)^2}} \right) \quad (4.3)$$

#### 4.1.2 Total horizontal derivative

In Cartesian coordinates, the total horizontal gradient (THG) of the gravity anomaly field  $g$  is defined by the relation (Nabighian, 1974; Roest *et al.*, 1992)

$$\text{THG} = \sqrt{\left(\frac{\partial g}{\partial x}\right)^2 + \left(\frac{\partial g}{\partial y}\right)^2 + \left(\frac{\partial g}{\partial z}\right)^2} \quad (4.4)$$

These filters are efficient to isolate boundaries, since maximum value usually is located above the source, especially when symmetry is present (Ghomsi *et al.*, 2022). The method was used here to highlight the deep geological setting which is assumed to be the sources of geothermal energy resources in the area.

#### 4.2 Spectral analysis of gravity data

Spectral analysis as described by Spector and Grant (1970), Dimitriadis *et al.* (1987), Fairhead and Okereke (1988), Bonvalot (1990), and Chakraborty and Agarwal (1992) is an interpretation technique based on the study of power spectrum properties. From the study of logarithmic power spectrum as a function of the spatial frequency, the mean depth of bodies responsible for the observed gravity anomalies can be estimated. The gravity data varies as a function of distance along a profile. The average depths of the source bodies responsible of the observed gravity anomalies are determined by using the

following expression by *Gerard and Debeglia* (1975)

$$d = \frac{\Delta \ln E(k)}{4\pi \Delta k}, \quad (4.5)$$

where  $\Delta \ln E(k)$  is the variation of the logarithm of the power spectrum for a wave number  $\Delta k$  ( $\text{rad/km}^{-1}$ ) and  $d$  (km) is the depth to approximate plane of density contrast. This relation is deduced from the power spectrum logarithm curve versus the wave number. On this curve, straight-line segments can be identified and plotted by a least square fitting on the data points. The high wave portion is due to shallow bodies. Deep-seated bodies cause the low wave number part.

### 4.3 3-D modeling and inversion of gravity sources

The 3-D inversion method used in this study was originally proposed by *Pirttijärvi* (2014). The forward computation is based on the dipping prism model algorithm (*Hjelt*, 1972) by inverting the gravity data. The method was evaluated and successfully found to determine the upper and lower crustal density structures (*Peace et al.*, 2018; *Welford et al.*, 2018). However, gravity data inversion has a non-unique solution as gravity anomalies result from the sum of all the gravity effects in the subsurface (*Skeels*, 1947; *Chakraborty and Agarwal*, 1992; *Strykowski*, 1998; *Widiwijayanti et al.*, 2004). In addition, the inversion modeling objective is to minimize the difference ( $e$ ) between measured gravity data ( $d_i$ ) and estimated gravity model responses ( $y_i$ ). The use of Grablox was based on a singular value decomposition (SVD), with adaptive damping used within unconstrained inversions. The root mean square (RMS) error between response and observations is written as follows (*Pirttijärvi*, 2014):

$$\text{RMS} = \sqrt{\frac{1}{M} \sum_{i=1}^M \left( \frac{d_i - y_i}{\Delta d} \right)^2} \quad (4.6)$$

where  $\Delta d$  is the difference between the maximum value ( $d_{\max}$ ) and the minimum value ( $d_{\min}$ ) of gravity anomaly used to scale the data. The inversion process was done repeatedly until a certain number of iterations to get a small difference ( $e$ ). In this study, spatial discretisation involved 25 west-east directed grid blocks, 25 north-south directed grid blocks and 10 grid blocks in the Z direction, so we reconstructed the initial model in the form of 6250 3-D minor blocks using Grablox. For three-dimensional gravity modeling and inversion, we used an interactive computer program for visualization and editing of large-scale 3-D models (Bloxer 1.6) and a gravity modeling and inversion software Grablox 2.1 based on a 3-D blocks model by *Pirttijärvi* (2003). The starting model was built up by approximate the entire region by  $29 \text{ km} \times 11 \text{ km} \times 5 \text{ km}$  blocks sizes. The initial density distribution was arbitrarily filled and progressively changed by means of a trial-and-error procedure using Grablox program to compute the gravity anomaly of the model and to compare it to the observed anomaly.

## 5 Results and discussion

### 5.1 Tilt derivative gravity

The advantages of tilt derivative gravity method compared to other is that it does not need parameters (density, magnetic susceptibility, inclination, deflection angle, permanent magnetization, and structural index). Due to the nature of the arc-tangent trigonometric function, all tilt amplitudes are restricted between  $-90^\circ$  and  $+90^\circ$  (Miller and Singh, 1994; Salem *et al.*, 2007, 2008). This map (Fig. 5.1a) shows the results obtained after applying the TDR to the gravity anomaly data. The map reveals that derivative yields a gravity configuration that emphasizes the linear trends in the gravity anomaly field and the distribution of tilt derivative values ranges from  $-1.30$  rad up to  $1.50$  rad. Value is positive for the source, zero value for the edge next to the source vertical and negative value for the other responses, where the edge of the source can be assumed as fault and rock density contrast (Putri *et al.*, 2019). We clearly see the concentration of tilt derivative high bounded by values close to zero in the southern part of the map, mainly along the faults with a longitude of 550 km to 460 km striking WNW–ESE. To highlight the structural directions shown on the TDR map, we drew the corresponding sketch map (Fig. 5.1b). This map shows a predominance of deep fractures provoked by the collision in cover. Fractures can be suspected preferential paths as the circulation of hydrothermal fluids.

### 5.2 Total horizontal gradient

Total horizontal gradient yields a gravity configuration that emphasizes the circular trends in the gravity anomaly field (Fig. 5.2). On this map, three circular trends are unveiled in the southern part near the deep fractures locality. The first one is formed by an interior ring of 150 km striking N–S. The second is associated to a circular ring with a longitude of 50 km striking E–W. The third trend at the end of the map is poorly defined. Results of this analysis give an overview of the possible deep geological setting in the area. By taking into account the tectonic setting of the northern margin of Congo Craton in Cameroon characterized by the presence of deep Precambrian faults, i.e., its limit with the Mobile Zone and the existence of a Cenozoic metamorphism represented by orthogneisses and gneisses, which had been subjected to medium-high pressure metamorphism reaching the granulite facies at depth during the Pan-African reactivation. These deep geological structures (granulites) are assumed to be the sources of geothermal energy resources in the area.

### 5.3 Spectral analysis of gravity data

After the description of the substantial gravity anomalies fields in the survey area, the question of depth to the sources of the gravity anomalies arises. One which can easily be applied to Bouguer anomaly map in this case is depth estimation by spectral analysis of gravity data. This figure (Fig. 5.3) shows the results obtained after applying the spectral analysis method. In this graph, the logarithm function of the power spectrum versus

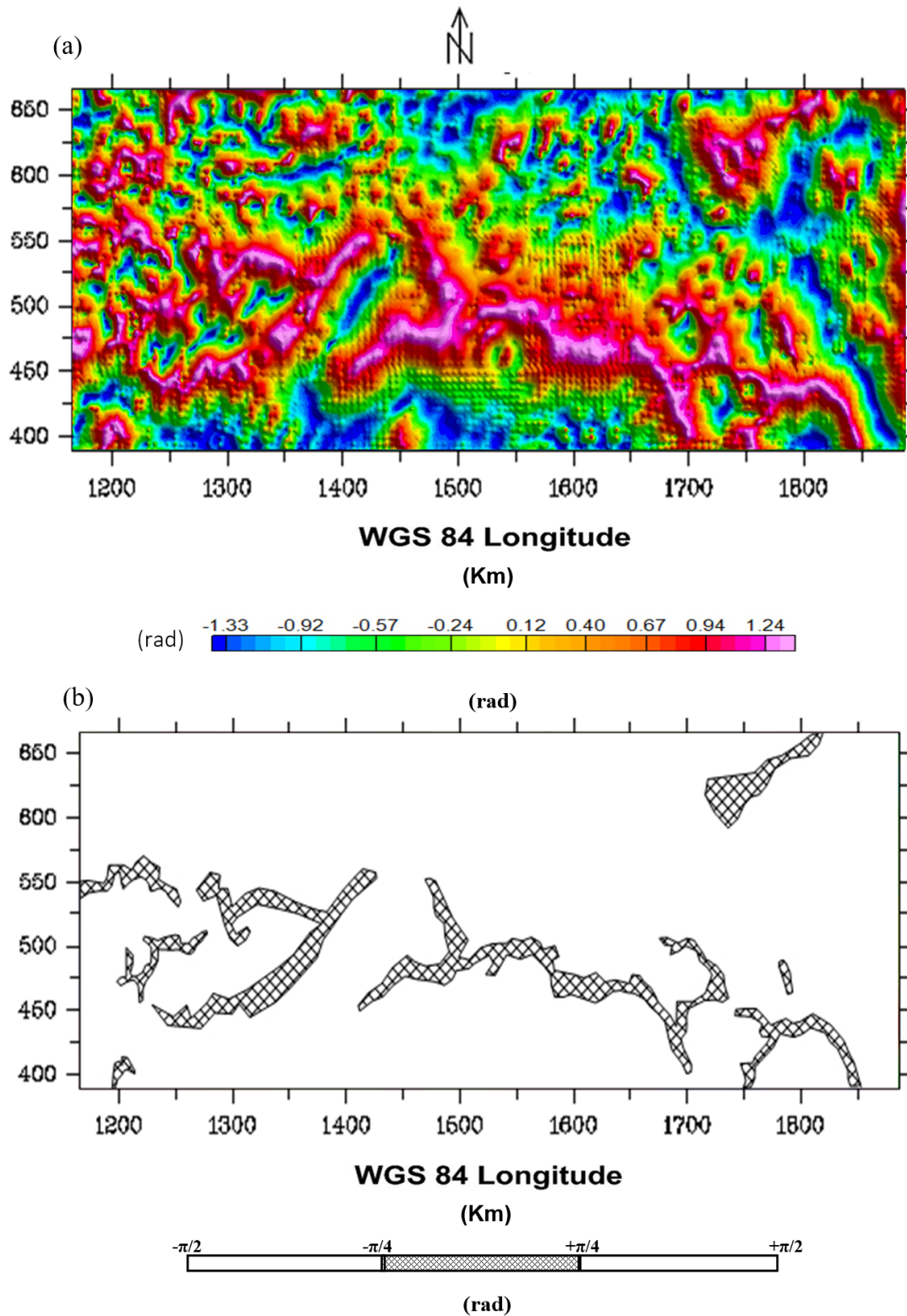


Fig. 5.1: (a) Shaded relief of tilt angle derivative (TDR) map of the studied area. (b) Sketch of the gravity sources and the faults system generated.

the wave number presents approximately three linear segments with different slopes. The slope of each segment divided by  $4\pi$  is a measure of the depths of the major discontinu-

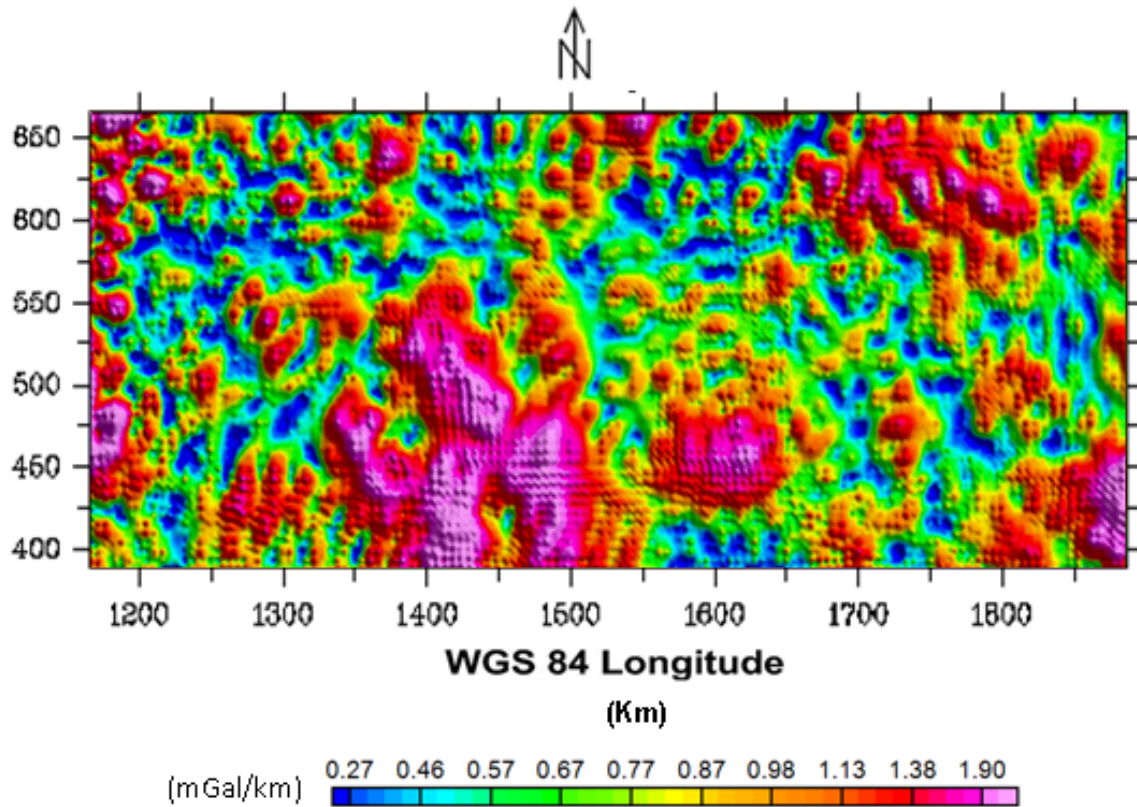


Fig. 5.2: Shaded relief of total horizontal derivative (THD) map of the studied area.

ities in the basement by means of Eq. (4.5). The first domain in the very low frequency ( $0.005 \text{ rad km}^{-1}$  to  $0.01 \text{ rad km}^{-1}$ ) has a depth of 50 km. This depth corresponds to the mean crustal thickness in the area. The second (28 km) and third (12 km) domains with frequency ranging from  $0.01 \text{ rad km}^{-1}$  to  $0.02 \text{ rad km}^{-1}$  and  $0.02 \text{ rad km}^{-1}$  to  $0.03 \text{ rad km}^{-1}$  respectively were assumed to be the depths of deep geological intrusions into the basement. Thus, the depth of 50 km was used in this study for 3-D modeling and inversion of gravity sources.

#### 5.4 3-D modeling and inversion of gravity sources

The identification of high gravity horizon in southern Cameroon by applying derivatives method encouraged the test of the result by building the 3-D model of distribution of density. Using a background density of  $2.670 \text{ g cm}^{-3}$ , the inversion process produces high negative to high positive contrast values of rock density between  $-0.670 \text{ g cm}^{-3}$  and  $+0.330 \text{ g cm}^{-3}$ . The root mean square (RMS) error generated from the data is 0.038, while that of the model is 0.00. These maps (Fig. 5.4a; 5.4b; 5.4c) show deviation from the inversion process (distribution of light blue and yellow) and the results of these analysis indicate that there is a high match between the observations and calculated data. The subsurface model was constructed in four horizontal layers at depths of 10 km, 30 km, 40 km, and 45 km (Fig. 5.5a; 5.5b; 5.5c). The first layer (10 km) shows a more homogeneous model dominated by rocks with negative to moderate positive contrast of density ( $-0.170 \text{ g cm}^{-3}$

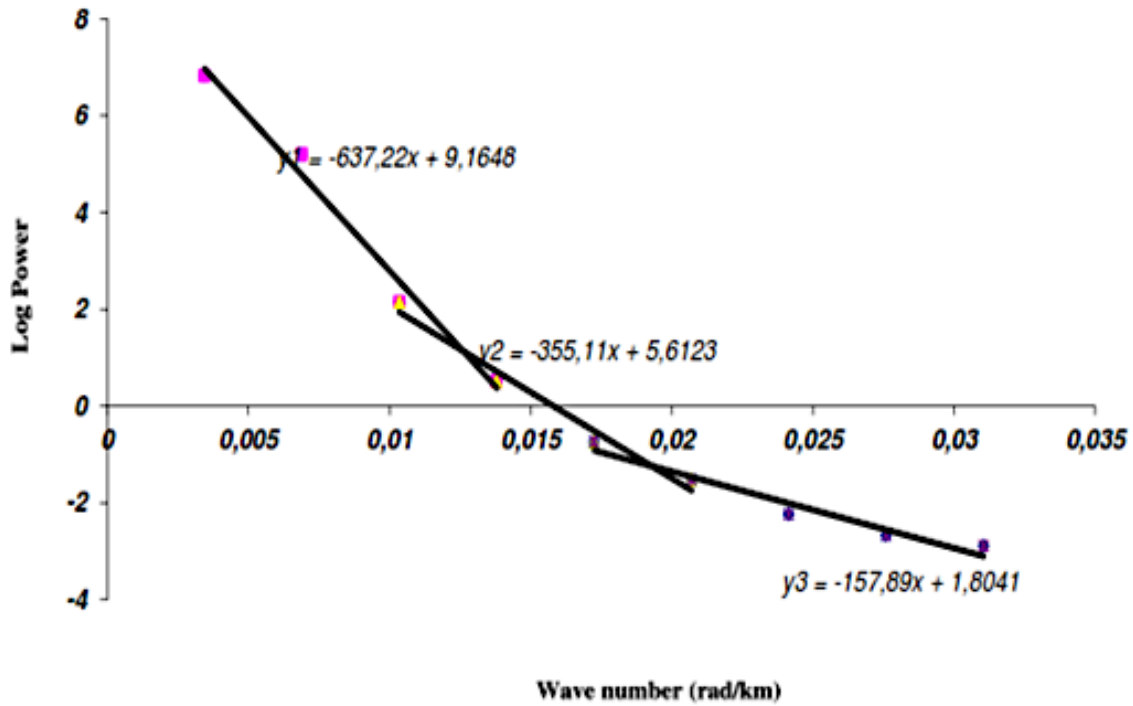


Fig. 5.3: Power spectrum for estimation of the top depths using the one-dimensional gravity anomaly data of the area. **50(a)**; **28(b)** and **12(c)** km are obtained as the Moho, intracrustal and the basement interface using the gradient of spectra defined as  $\Delta \ln(k)/4\pi\Delta k$ , where  $\Delta k$  is the wave number and  $\Delta \ln(k)$  is the radially averaged power spectrum energy.

to  $+0.130 \text{ g cm}^{-3}$ ). The second layer (30 km) is dominated by rocks with negative to high positive contrast of density ( $-0.300 \text{ g cm}^{-3}$  to  $+0.330 \text{ g cm}^{-3}$ ). This layer looks more complex with high positive contrast of density in the south and high negative in the northern part of the area. The third (40 km) and fourth (45 km) layers, which are dominated by rock with high negative to high positive contrasts of density, having values ranging from  $-0.470 \text{ g cm}^{-3}$  to  $+0.230 \text{ g cm}^{-3}$  and  $-0.670 \text{ g cm}^{-3}$  to  $+0.180 \text{ g cm}^{-3}$  respectively. To reinforce the prediction of possible deep geological setting in the area, we constructed four vertical 3-D density-models across the zone of faults each of one west-east trending direction and three south-north-trending direction.

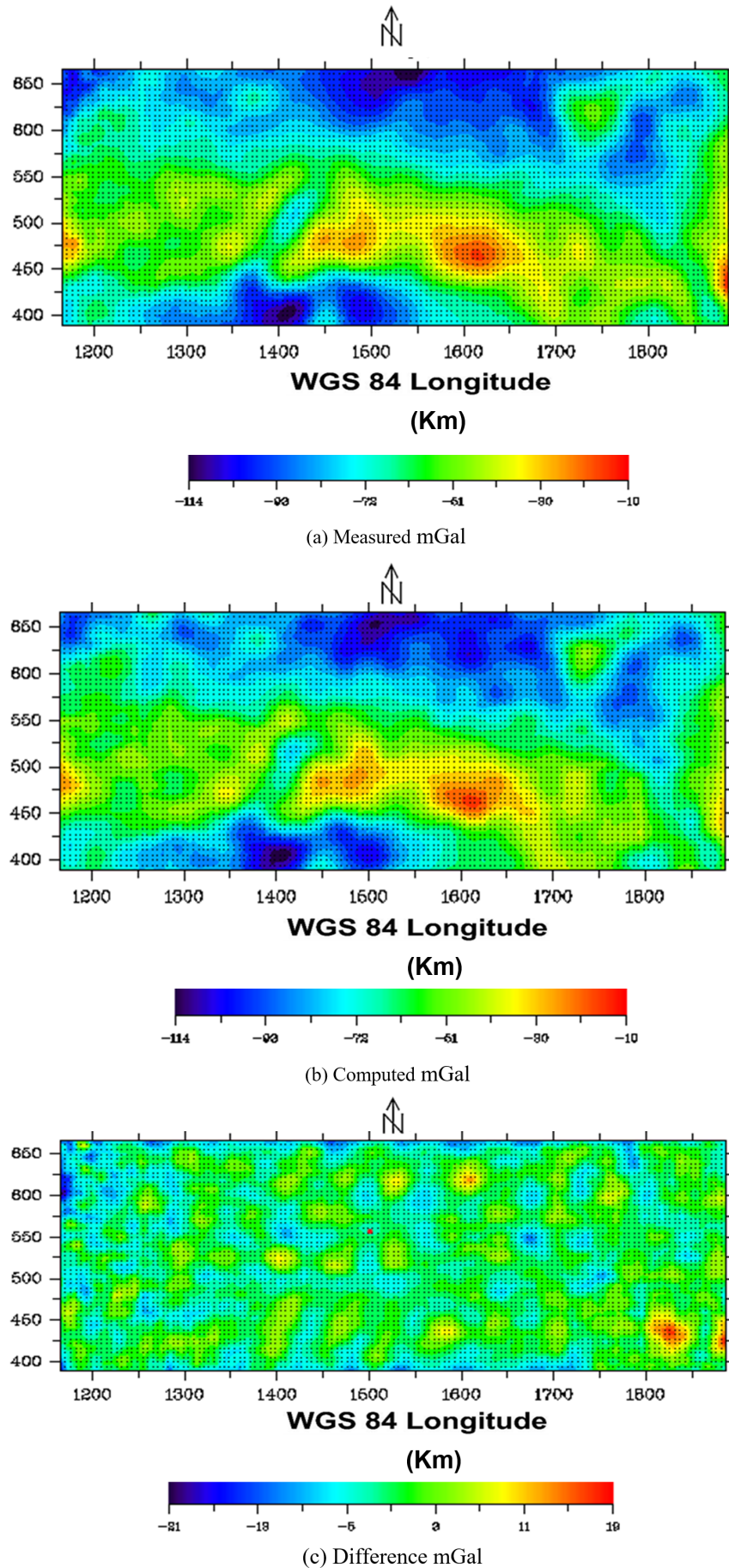
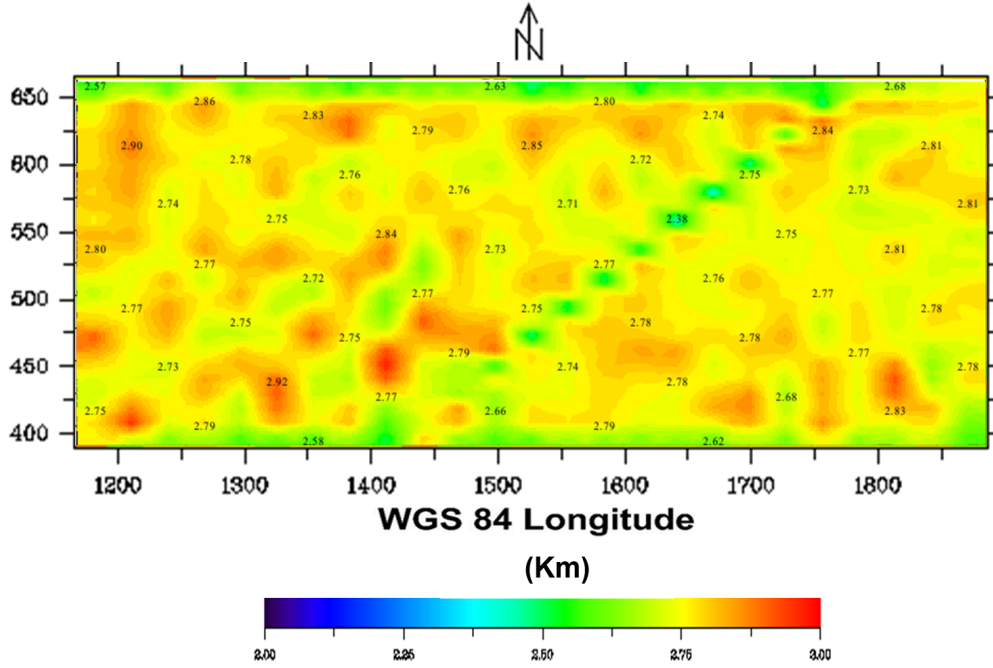
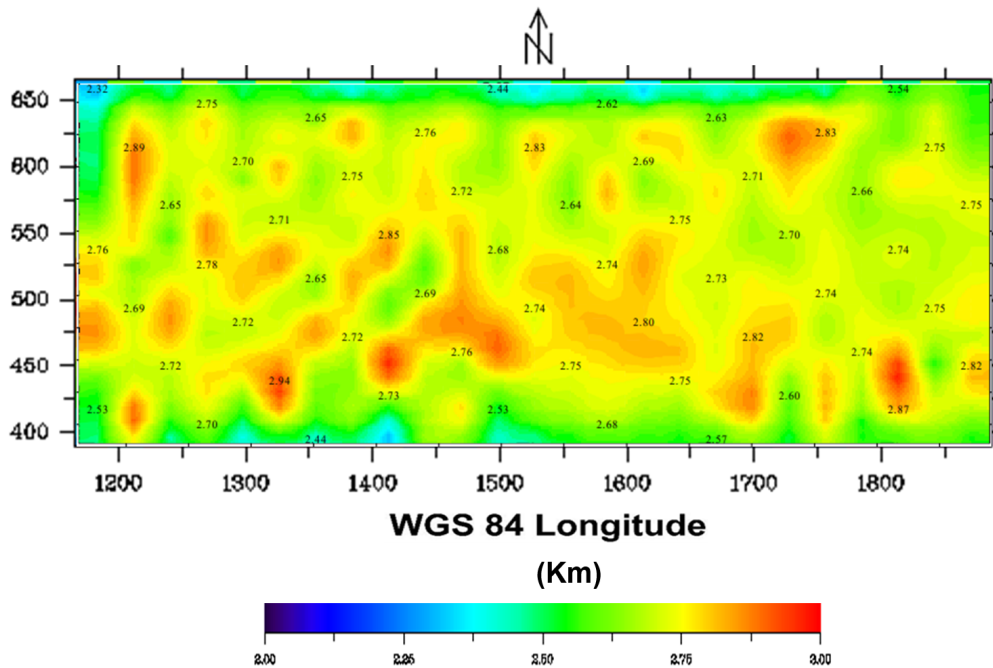


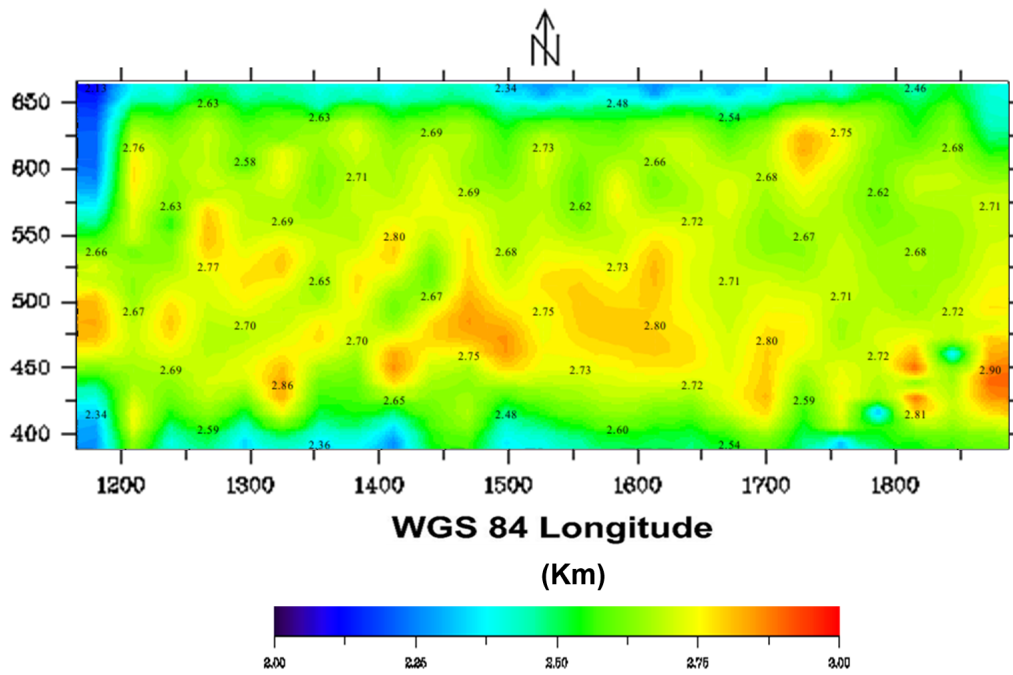
Fig. 5.4: 3-D density inversion of gravity data result beneath the studied area: (a) Measured data; (b) Computed data and (c) Error of the inversion.



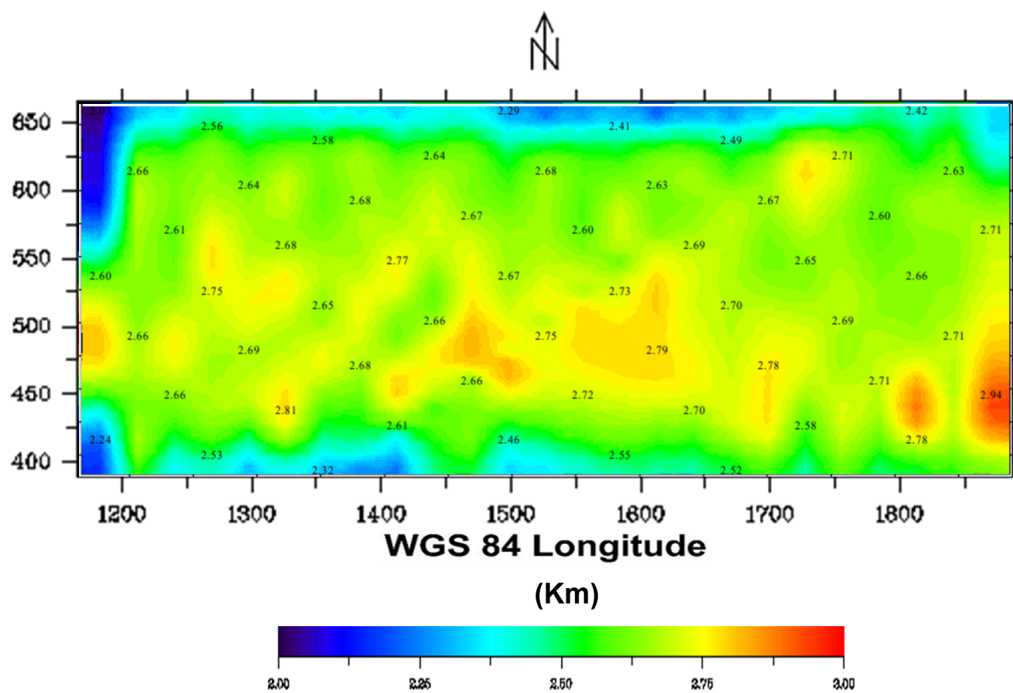
(a) Density at 10km  $g/cm^3$



(b) Density at 30km  $g/cm^3$



(c) Density at 40km g/cm<sup>3</sup>



(d) Density at 45km g/cm<sup>3</sup>

Fig. 5.5: 3-D subsurface model of Pan-Africa belt and Congo Craton based on gravity data inversion at depth of (a) 10 km; (b) 30 km; (c) 40 km; (d) 45 km.

### 5.4.1 North–South 3-D density models

The North-South 3-D density models were chosen to include major negatives gravity anomalies on both sides of the positives gravity anomalies interpreted as a zone of faults (see Fig. 3.2). It can be seen that, the three verticals cross sections directed North–South shows a massive and evident intrusion pattern with high rock density contrast, are displayed in Fig. 5.6a; Fig.5.6b and Fig.5.6c. The highest density intrusion is well represented in the southern part of the models, down to a depth of 20 km with enough high positive contrast of density ( $+0.33 \text{ g cm}^{-3}$ ). The prediction of massive igneous rock intrusions occurred just below the zone of faults in the southern part of the Bouguer map and its surroundings. This deep geological setting probably granulitic rock put in place at the zone of collision during the Pan-Africa reactivation was assumed to be the source of geothermal energy resources in the area.

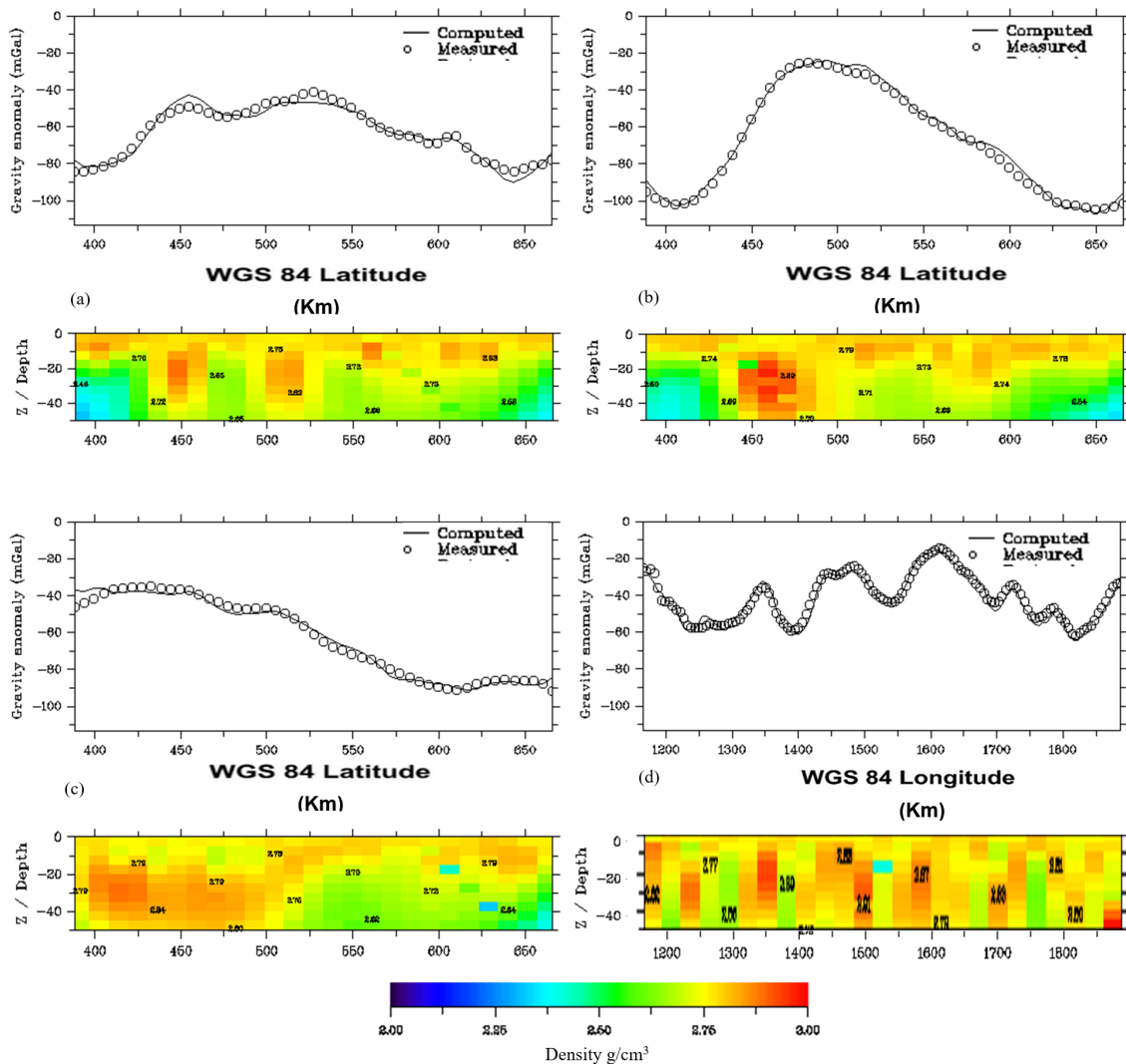


Fig. 5.6: Profiles and cross-sections of the subsurface density of Pan-Africa belt and Congo Craton boundary, Centre–South Cameroon (a), (b) and (c) from north to south and (d) from west to east. In the upper box are shown the measured and calculated gravity anomalies.

#### 5.4.2 West–East 3-D density models

The selection of one vertical cross section directed West-East for 3-D modeling was motivated by the results of the prior North-South models. This 3-D density model was chosen to fully include the high positive gravity anomalies on the Bouguer map in Fig. 3.2. Results of this analysis (Fig. 5.6d) clearly give an overview of the presence of deep geological setting in the area with high positives contrast of density, which crosses the area from West to East.

### 6 Geothermal implications

The interpretative 3-D density models cross sections of the studied area (Fig. 5.6a; Fig. 5.6b; Fig. 5.6c and Fig. 5.6d) clearly give an overview of the presence of deep geological setting probably granulitic rocks put in place at the zone of faults during the Pan-African reactivation in the southern part. This result can therefore help us to:

- Locate the position for existence of faults. Faults can be suspected preferential paths as the circulation of hydrothermal fluids.
- Map the zone of deep geological setting with high density in the area. High intrusives density are acting as the sources of geothermal energy resources.

### 7 Conclusion

In this study, Geothermal energy resources of the northern part of Congo Craton boundary in Cameroon are highlighted by 3-D geophysical inversion-modeling and intrusion estimation using gravity data. The magnitude maxima of (1) tilt derivative gravity and (2) the total horizontal gradient allowed maps to be produced showing various lines of fractures and deep geological setting in the area. These structures are associated to long-wavelength anomalies, suggesting that its should be connected with large-scale structural deformation due to the collision between Congo Craton (CC) and Pan-African belt or Mobile zone (MZ) and constitutes the preferential paths of circulation of hydrothermal fluids up flow to the surface. Interpretative 3-D density models show the distribution of high density associated to deep geological structures probably granulitic rocks put in place near faults and surroundings. High density intrusions are acting as the source of geothermal energy resources in the area. This study can be considered as preliminary research aiming to improve our knowledge about the geothermal regime of this complicated region as this area requires substantially more thermal data.

#### *Declaration of competing interest*

There is no conflict of interest on this article entitled “3D geophysical inversion-modeling and intrusion estimation using gravity data of convergence zone between Pan-African-belt and Congo Craton, Centre-South of Cameroon: its implications on limit between the two geotectonic units”.

### Acknowledgement

The authors thank Mr. Pirttijärvi, who developed an interactive computer program for visualization and editing of large-scale 3-D model Bloxer 1.6 and a gravity modeling and inversion software Grablox 2.1 based on a 3-D blocks model and Mr. Kari Moisis is thanked for his detailed and constructive reviews that improved the quality of this manuscript.

### References

- Abdelsalam, G. M., L. Liégeois and R. J. Stern, 2002. The Saharan Metacraton. *Journal of African Earth Sciences*, **34**, 119–136.
- Andersson, M. and A. Malehmir, 2018. Internal architecture of the Alnö alkaline and carbonatite complex (central Sweden) revealed using 3D models of gravity and magnetic data. *Tectonophysics*, **740–741**, 53–71. DOI: 10.1016/j.tecto.2018.05.008.
- Bonvalot, S., 1990. “Mesures gravimétriques en Guinée et en Sierra-Léone. Modélisation structurale et étude du comportement mécanique de la lithosphère: étude d’une chaîne péricratonique, d’un bombement intraplaque et de marges transformantes”. PhD thesis. Université Paris VI.
- Caron, V., E. Ekomane, G. Mahieux, P. Moussango and E. Ndjeng, 2010. The Mintom formation (new): Sedimentology and geochemistry of neoproterozoic, paralic succession in south-east Cameroon. *Journal of African Earth Sciences*, **57**, 367–385.
- Chakraborty, K. and B. N. P. Agarwal, 1992. Mapping of crustal discontinuities by wavelength filtering of the gravity field. *Geophysical Prospecting*, **40**, 801–822.
- Choi, S., I.-C. Ryu and Y.-C. Lee, 2019. An analysis of the intraplate earthquake (2016M5.8.GY) that occurred in the Gyeongsang Basin in the SE of the Korean Peninsula, based on 3-D modeling of the gravity and magnetic field. *Geophysical Journal International*, **217** (1), 90–107. DOI: 10.1093/gji/ggz001.
- Collignon, F., 1968. *Gravimétrie et reconnaissance de la République Fédérale du Cameroun*. Paris: ORSTOM. 35 pp.
- Cooper, G. and D. Cowan, 2006. Enhancing potential field data using filters based on the local phase. *Computers & Geosciences*, **32** (10), 1585–1591. DOI: 10.1016/j.cageo.2006.02.016.
- Crenn, Y., 1967. Mesures gravimétriques et magnétiques dans la partie centrale de l’AOF. Interprétation géologique. Tech. rep. Publi série géophys. Paris, France: ORSTOM. 43 pp.
- Dimitriadis, K., G.-A. Tselentis and K. Thanassoulas, 1987. A basic program for 2-D spectral analysis of gravity data and source depth estimation. *Computers & Geosciences*, **13** (5), 549–560.
- Fairhead, D. and C. S. Okereke, 1988. Depths to major density contrasts beneath the West-African rift system in Nigeria and Cameroon based on the spectral analysis of gravity data. *Journal of African Earth Sciences*, **7** (5–6), 769–777.

- Farhi, W., A. Boudella, H. Saibi and M. O. A. Bounif, 2016. Integration magnetic, gravity and well data in imaging subsurface geology in the Ksar Hirane region (Laghouat, Algeria). *Journal of African Earth Sciences*, **124**, 63–74. DOI: 10.1016/j.jafrearsci.2016.09.013.
- Feumoe, Alain Narcisse S., 2014. “Apport des filtrages et inversions  $2D^{1/2}$  des anomalies aéromagnétiques dans la détermination des accidents tectoniques majeurs au Sud-est du Cameroun (Craton du Congo)”. PhD thesis. Université de Yaoundé I. 154 pp.
- Feumoe, Alain Narcisse S. and T. Ndougsa-Mbarga, 2017. Curie point depth variations derived from aeromagnetic data and the thermal structure of the crust at the zone of continental collision (south-eastern Cameroon). *Geophysica*, **52** (1), 31–45.
- Feumoe, Alain Narcisse S., T. Ndougsa-Mbarga, E. Manguelle-Dicoum and J. D. Fairhead, 2012. Delineation of tectonic lineaments using aeromagnetic data for the south-east Cameroon area. *Geofizika*, **29**, 175–192.
- Geng, M., M. Y. Ali, J. D. Fairhead, Y. Bouzidi and B. Barkat, 2020. Morphology of the basement and hormuz salt distribution in offshore Abu Dhabi from constrained 3D inversion gravity and magnetic data. *Tectonophysics*, **791**, 228563. DOI: 10.1016/j.tecto.2020.228563.
- Geng, M., J. K. Welford, C. G. Farquharson and X. Hu, 2019a. Gravity modeling for crustal-scale models of rifted continental margins using a constrained 3D inversion method. *Geophysics*, **84** (4), G25–G36. DOI: 10.1191/geo.2018-01.34.1.
- Geng, M., J. K. Welford, C. G. Farquharson and L. Pease, 2019b. 3D inversion of airborne gravity gradiometry data for the Budgell Harbour Stock, Newfoundland: A case history using a probabilistic approach. *Geophysics*, **84** (4), B269–B284. DOI: 10.1190/geo.2018-0407.1.
- Gerard, A. and N. Debeglia, 1975. Automatic three-dimensional modeling for interpretation of gravity or magnetic anomalies. *Geophysics*, **40**, 1014–1034.
- Ghoms, Franck Eitel Kemgang, Janvier Domra, K. Zakari Aretouyap, Nelson Ribeiro-Filho, Luanh Pham, Raissa Baldez, Robert Tenzer, Animesh Mandal and Alain Nzeuga, 2022. Main structural lineaments of the southern Cameroon volcanic line derived from aeromagnetic data. *Journal of African Earth Sciences*, **186**, 104418. DOI: 10.1016/j.jafrearsci.2021.104418.
- Ghoms, Franck Eitel Kemgang, Cristiano Mendel Martins, Nelson Ribeiro-Filho, Raissa Baldez, Robert Tenzer, Chikondi Chisenga, Severin Nguiya and Robert Nouayou, 2020. Identification of Cameroon’s geological structures through a gravity separation and using seismic crustal models. *Journal of African Earth Sciences*, **173**, 104027. DOI: 10.1016/j.jafrearsci.2020.104027.
- Gunn, P. J., 1975. Linear transformations of gravity and magnetic fields. *Geophysical Prospecting*, **23**, 300–312.
- Hjelt, Sven-E., 1972. Magnetostatic anomalies of dipping prisms. *Geoexploration*, **10**, 239–254.
- Kennedy, W. Q., 1984. “The structural differentiation of Africa in the Pan African 500 Ma tectonic episode”. In: *8<sup>th</sup> Ann. Rep. Res. Inst. Afr. Géol.* Leeds University, U. K., 48–49.

- Manguelle Dicoum, E., A. S. Bokosah and T. E. Kwende Mbanwi, 1992. Geophysical evidence for a major Precambrian schist-granite boundary in southern Cameroon. *Tectonophysics*, **205**, 437–446.
- Maurizot, P., A. Abessolo, J. Feybesse, L. Johan and P. Lecomte, 1986. Etude et prospection minière du Sud-Ouest du Cameroun. Synthèse des travaux de 1978 à 1985. Tech. rep. 85. CMR 066. Orleans: Rapport BRGM. 274 pp.
- Mbom-Abane, S., 1997. “Investigations géophysiques en bordure du craton du Congo (région d’Abong Mbang / Akonolinga, Cameroun) et implications structurales”. PhD thesis. Université de Yaoundé I. 180 pp.
- Miller, H. G. and V. Singh, 1994. Potential field tilt a new concept for location of potential field sources. *J. Appl. Geophys.*, **32**, 213–217. DOI: 10.1016/0926-9851(94)90022-1.
- Moghaddam, M. M., S. Mirzaei, J. Nouraliee and S. Porkhial, 2016. Integrated magnetic and gravity surveys for geothermal exploration in Central Iran. *Arabian Journal of Geosciences*, **9**(7), 1–12.
- Mvondo, H., S. W. J. Den-Brok and J. Mvondo-Ondoa, 2003. Evidence for symmetric extension and exhumation of the Yaoundé nappe (Pan-African fold Belt, Cameroon). *J. Afr. Earth Sci.*, **35**, 215–231.
- Nabighian, M. N., 1974. The analytic signal of two-dimensional magnetic bodies with polygonal cross-section: its properties and use for automated anomaly interpretation. *Geophysics*, **37**, 507–517.
- Ndougsa-Mbarga, T., N. A. S. Feumoe, E. Manguelle-Dicoum and J. D. Fairhead, 2012. Aeromagnetic Data Interpretation to Locate Buried Faults in South-East Cameroon. *Geophysica*, **48**(1–2), 49–63.
- Ngako, V., P. Affaton, J. M. Nnange and T. Njanko, 2003. Pan-African tectonic evolution in central and southern Cameroon: transpression and transtension during sinistral shear movements. *Journal of African Earth Sciences*, **36**(3), 207–214.
- Nouraliee, J., S. Porkhial, M. M. Moghaddam, S. Mirzaei, D. Ebrahimi and M. R. Rahmani, 2015. Investigation of density contrasts and geologic structures of hot springs in the Markazi Province of Iran using the gravity method. *Russian Geology and Geophysics*, **56**(12), 1791–1800.
- Nzenti, J. P., P. Barbey, J. Macaudière and D. Soba, 1988. Origin and evolution of the late Precambrian high-grade Yaoundé gneisses (Cameroon). *Precambrian Research*, **38**, 91–109.
- Owona, S. M., S. P. Ndzana and O. J. Mvondo, 2012. Geological control of geomorphologic units in the Southwest (SW) Cameroon (Central Africa). *Journal of Geology and Mining Research*, **4**(7), 152–167.
- Peace, A. L., J. K. Welford, M. Geng, H. Sandeman, B. D. Gaetz and S. S. Ryan, 2018. Rift-related magmatism on magma-poor margins: Structural and potential-field analyses of the Mesozoic Notre Dame Bay intrusions, Newfoundland, Canada and their link to North Atlantic Opening. *Tectonophysics*, **745**, 24–45. DOI: 10.1016/j.tecto.2018.07.025.

- Pirttijärvi, M., 2003. *GRABLOX Gravity interpretation and modeling software based on 3D block models. User's guide to version 2.1.*
- Pirttijärvi, M., 2014. *GRABLOX 2.1. Gravity Interpretation and Modelling Using 3D Block Models, User's Guide to Version 2.1.* Oulu, Finland.
- Poidevin, J. L., 1983. "La tectonique Pan-Africaine à la bordure nord du craton congolais : l'orogénèse des Oubanguides". In: *Colloque on the African geology*. Musée Royal de l'Afrique centrale, Tervuren, Belgium.
- Poidevin, J. L., 1991. "Les ceintures des roches vertes de la RCA. Contribution à la connaissance du précambrien du Nord du Craton du Congo". Thèse Doct. Sic. Univ. Clermont Fernand.
- Putri, D. R., M. Nanda, S. Rizal, R. Idroes and N. Ismail, 2019. Interpretation of gravity satellite data to delineate structural features connected to geothermal resources at Bur Ni Geureudong geothermal field. *IOP Conf. Series: Earth and Environmental Science*, **364**, 012003.
- Roest, W. R., J. Verhoef and M. Pilkington, 1992. Magnetic interpretation using the 3-D analytic signal. *Geophysics*, **57**, 116–125. DOI: 10.1190/1.1443174.
- Salem, A., S. Williams, D. Fairhead, D. Ravat and R. Smith, 2007. Tilt-depth method: A simple depth estimation method using first-order magnetic derivatives. *The Leading Edge*, **26** (12), 1502–1505.
- Salem, A., S. Williams, D. Fairhead, D. Ravat, R. Smith and D. Ravat, 2008. Interpretation of magnetic data tilt-angle derivatives. *Geophysics*, **73**, L1–L10.
- Shandini, N. Y., J. M. Tadjou and C. A. Basseka, 2011. Delineating deep basement faults in South Cameroon area. *World Applied Sciences Journal*, **14** (4), 611–615.
- Shandini, N. Y., J. M. Tadjou, C. T. Tabod and J. D. Fairhead, 2010. Gravity data interpretation in the northern edge of the Congo Craton, South-Cameroon. *Anuário do Instituto de Geociências*, **33** (1), 73–82.
- Skeels, D. C., 1947. Ambiguity in gravity interpretation. *Geophysics*, **12**, 43–56.
- Soba, D., 1989. "La série du Lom : étude géologique et géochronologique d'un bassin volcano-sédimentaire de la chaîne panafricaine de l'Est du Cameroun". Thèse d'État. Université Paris VI. 181 pp.
- Spector, A. and F. S. Grant, 1970. Statistical models for interpreting aeromagnetic data. *Geophysics*, **35**, 293–302.
- Strykowski, G., 1998. Experiences with a detailed estimation of the mass density contrasts and of the regional gravity field using geometrical information from seismograms. *Phys. Chem. Earth*, **23** (9–10), 845–856.
- Tadjou, J. M., E. Manguelle-Dicoum, C. T. Tabod, R. Nouayou, J. Kamguia, N. P. Njandjock and M. T. Ndougsa, 2004. Gravity modelling along the northern margin of the Congo craton, South-Cameroon. *J. Cameroon Acad. Sci.*, **4**, 51–60.
- Tadjou, J. M., R. Nouayou, J. Kamguia, H. L. Kande and E. Manguelle-Dicoum, 2009. Gravity analysis of the boundary between the Congo craton and the Pan-African belt of Cameroon. *Austrian Journal of Earth Sciences*, **102** (1), 71–79.

- Tchameni, R., 2001. Crustal origin of Early Proterozoic syenites in the Congo Craton (Ntem Complex), South Cameroon. *Lithos*, **57** (1), 23–42.
- Tchameni, R., K. Mezger, E. Nsifa and A. Pouclet, 2000. Neoarchean evolution in the Congo Craton: evidence from K-rich granitoids of the Ntem Complex, Southern Cameroon. *J. Afr. Earth Sci.*, **30**, 133–147.
- Telford, W. M., L. P. Geldart and R. E. Sheriff, 1990. *Applied Geophysics*. Cambridge University Press. DOI: 10.1017/cbo9781139167932.
- Tokam, A. P. K., C. T. Tabod, A. A. Nyblade, J. Julia, D. A. Wiens and M. E. Pasyanos, 2010. Structure of the crust beneath Cameroon, West Africa from the joint inversion of Rayleigh wave group velocities and receiver functions. *Geophys. J. Int.*, **183**, 1061–1076.
- Toteu, S. F., J. Penaye and Y. D. Poudjom, 2004. Geodynamic evolution of the Pan-African belt in central Africa with special reference to Cameroon. *Canadian Journal of Earth Sciences*, **41**, 73–85.
- Toteu, S. F., R. W. Van Schmus, J. Penaye and A. Michard, 2001. New U–Pb and Sm–Nd data from north-central Cameroon and its bearing on the pre-Pan-African history of central Africa. *Precambrian Research*, **108**, 45–73.
- Toteu, S. F., W. R. Van Schmus, J. Penaye and J. B. Nyobe, 1994. U–Pb and Sm–Nd evidence for Eburnean and pan-African high-grade metamorphism in cratonic rocks of southern Cameroon. *Precambrian Res.*, **67**, 321–347.
- Verduzco, B., J. D. Fairhead, C. M. Green and C. MacKenzie, 2004. New insights into magnetic derivatives for structural mapping. *The Leading Edge*, **23**, 116–119.
- Vicat, J. P., 1998. “Esquisse géologique du Cameroun”. In: *Géosciences au Cameroun*. Vol. 1/1998. Collection GEOCAM, 3–11.
- Welford, J. K., A. L. Peace, M. Geng, S. A. Dehler and K. Dickie, 2018. Crustal structure of Baffin Bay from constrained three-dimensional gravity inversion and deformable plate tectonic models. *Geophysical Journal International*, **214** (2), 1281–1300. DOI: 10.1093/gji/ggy197.
- Widiwijayanti, C., C. Tiberi, C. Deplus, M. Diament and V. Mikhailov, 2004. Geodynamic evolution of the northern Molucca Sea area (Eastern Indonesia) constrained by 3D gravity field inversion. *Tectonophysics*, **386**, 203–222. DOI: 10.1016/j.tecto.2004.05.003.